Quantum Modelling of Magnetism in Strongly Correlated Materials: Evaluating Constrained DFT and LDA+U+J for Y114

Christian Tantardini[a,*], Darina Fazylbekova[a], Sergey Levchenko[b], Ivan S. Novikov[b,c,d]

[a]*Institute of Solid State Chemistry and Mechanochemistry SB RAS, 630128, Novosibirsk, Russian Federation,*
[b]*Skolkovo Institute of Science and Technology, Skolkovo Innovation Center, Bolshoy boulevard 30, Moscow, 121205, Russian Federation,*
[c]*Moscow Institute of Physics and Technology, 9 Institutskiy per., Dolgoprudny, Moscow Region, 141701, Russian Federation,*
[d]*Emanuel Institute of Biochemical Physics RAS, 4 Kosygin Street, Moscow, 119334, Russian Federation,*

Abstract

Transition-metal compounds represent a fascinating playground for exploring the intricate relationship between structural distortions, electronic properties, and magnetic behaviour, holding significant promise for technological advancements. Among these compounds, YBaCo$_4$O$_7$ (Y114) is attractive due to its manifestation of a ferrimagnetic component at low temperature intertwined with distortion effect due to the charge disproportionation on Co ions, exerting profound impact on its magnetic properties. In this perspective paper, we study the structural and magnetic intricacies of the Y114 crystal. Traditionally, the investigation of such materials has relied heavily on computational modelling using density-functional theory (DFT) with the on-site Coulomb interaction correction U (DFT+U) based on the Hubbard model (sometimes including Hund's exchange coupling parameter J, DFT+U+J) to unravel their complexities. Herein, we analysed the spurious effects of magnetic-moment delocalisation and spillover to non-magnetic ions in the lattice on electronic structure and magnetic properties of Y114. To overcome this problem we have applied constrained DFT (cDFT) based on the potential self-consistency approach, and comprehensively explore the Y114 crystal's characteristics in its ferrimagnetic order. We find that cDFT yields magnetic moments of Co ions much closer to the experimental values than LDA+U+J with the parameters U and J fitted to reproduce experimental lattice constants. cDFT allows for an accurate prediction of magnetic properties using oxidation states of magnetic ions as well-defined parameters. Through this perspective, we not only enhance our understanding of the magnetic interactions in Y114 crystal, but also pave the way for future investigations into magnetic materials.

1. Introduction

Co-containing oxides often possess interesting magnetic properties. Among them, YBaCo$_4$O$_7$ (abbreviated as Y114) has recently attracted attention [1, 2, 3, 4, 5] due to its complex magnetic behaviour. For example, this structure demonstrates a spin–glass transition at around 66 K from a high-temperature paramagnetic state [1, 2, 3, 4, 5]. In such materials, charge disproportionation can occur, which can strongly influence their magnetic properties. Based on the formal oxidation state count, in Y114 three Co ions per primitive unit cell must adopt +2 oxidation state, and one Co ion adopts a +3 oxidation state. Such materials are known to exhibit dynamic distortion due to electronic fluctuations between the Co ions [1, 2, 3, 4, 5]. For this reason, a direct experimental observation of the expected differences in oxygen tetrahedral environments for each unique cobalt site to assign the correct oxidation state is currently not feasible [1, 2, 3, 4, 5]. The inability to refine the structure experimentally due to dynamic distortion can be effectively addressed through a computational approach, as previously demonstrated by Tantardini *et al.* [6] using density-functional theory (DFT) in local density approximation (LDA) combined with the Hubbard on-site correction U (LDA+U). However, describing magnetism with Hubbard-model-based corrections may not be sufficient due to the lack of experimental data needed to determine the parameters of the model, the Hubbard U and Hund's coupling J, which describe the long-range interactions affecting local magnetic moments.

Here, we investigate the limitations of DFT+U+J in describing complex magnetic materials, and explain how such materials can be theoretically treated using constrained DFT (cDFT) based on the potential self-consistency approach [7]. This approach differs from previously developed cDFT methods [8, 9, 10], because it imposes charge or magnetic moment constraints by finding such a potential that the corresponding self-consistent wavefunctions and electronic density satisfy the constraints exactly, rather than by using a penalty function directly for the deviation of the constrained quantity from the target. Specifically, a Lagrangian potential-based self-consistency constraint [7] will be applied to model cobalt ions in different oxidation states, Co^{2+} and Co^{3+}, in Y114. Additionally, the same type of constraint is applied to the magnetic moments of other atoms in the lattice to prevent the spreading of magnetic moments to non-magnetic atoms, such as oxygen.

In summary, this study adopts an interdisciplinary approach, integrating experimental data obtained by inverse magnetic susceptibility measurement in X-ray powder diffraction at 2 K [5] and advanced computational techniques — specifically leverag-
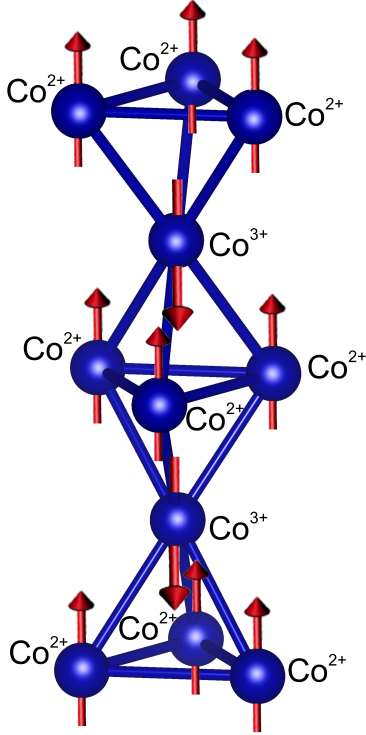
*Correspond to christiantantardini@ymail.com

Figure 1: Crystal structure of Y114 with Co^{2+} and Co^{3+} in their ferrimagnetic configuration.

ing cDFT with a constrained atomic charge and magnetic moments — to unravel the intricate structural, electronic, and magnetic properties of magnetic oxides, emphasising the impact of the dynamic distortions due to the chemical disproportionation on magnetic order preferences.

2. Theory

We aim to provide a comparison between DFT+U+J and cDFT for describing strongly correlated materials [11]. In Kohn-Sham (KS) DFT the electronic structure of a material is obtained by solving a system of single-particle equations known as KS equations. The Hamiltonian in these equations includes the sum of kinetic energy and the external potential of a single electron. To these terms, the Hartree term, representing the Coulomb repulsion between all electrons (including the spurious self-interaction), and the exchange-correlation term, approximated in various forms in DFT (e.g., LDA as considered here), are added. The KS states $\psi_{k,\nu}$ describe the single electron within a specific band ν at a specific k-point in the reciprocal space. These states are delocalized over the crystal.

In most cases, such a model can fully describe the properties of materials. However, in the case of strongly correlated materials such as transition-metal compounds, the self-interaction error and other exchange-correlation errors in approximate energy-functionals can lead to qualitatively incorrect description of localised valence d-orbitals, making it challenging to model oxidation states and magnetic interactions of transition-metal ions in crystals. The same problem occurs in

lanthanides and actinides with the localised f-orbitals. Over the years, the DFT+U model [12, 13, 14] in DFT practically addressed this issue by considering specific electronic interactions between atomic orbitals. Two alternative formulations avoiding the double counting (E^{dc}) are fully localised limit (FLL) [15] and around mean-field (AMF) [16]. The total energy in DFT+U is formulated as follows:

$$E^{\text{LDA}+U}[\rho, n] = E^{\text{LDA}}[\rho] + E^U[n] - E^{dc}[n]. \quad (1)$$

Here, ρ is the electron density of the system, while n is the density matrix for localised atomic orbitals on a specific atom A. This density matrix is generated by projecting KS states onto atomic orbitals with specific angular momentum ℓ and associated momentum projection m of the atom A:

$$n_{mm'}^{A\sigma} = \sum_{k,\nu} f_{k\nu}^\sigma \langle \varphi_m^{A\sigma} | \psi_{k,\nu} \rangle \langle \psi_{k,\nu} | \varphi_{m'}^{A\sigma} \rangle, \quad (2)$$

where f is the Fermi-Dirac distribution, σ is the spin on the atom A, and φ are the atomic orbitals described as product of radial functions and spherical harmonics centered on the atoms. If only diagonal terms of the local density matrix $n_{mm'}^{A\sigma}$ are considered, the term $E^U[n]$ will lose its invariance under rotation. Therefore, the terms that come from the off-diagonal local density matrix should be also considered.

The energy term in the Hubbard model ($E^U[n]$) is given by:

$$\begin{aligned} E^U[n] = \frac{1}{2} \sum_{A=1}^M \sum_{\{m\},\sigma} &\left\{ \left\langle \varphi_m^A, \varphi_{m''}^A \middle| V_{ee} \middle| \varphi_{m'}^A, \varphi_{m'''}^A \right\rangle n_{mm'}^\sigma n_{m''m'''}^{-\sigma} \right. \\ &+ \left(\left\langle \varphi_m^A, \varphi_{m''}^A \middle| V_{ee} \middle| \varphi_{m'}^A, \varphi_{m'''}^A \right\rangle \right. \\ &- \left. \left. \left\langle \varphi_m^A, \varphi_{m''}^A \middle| V_{ee} \middle| \varphi_{m'''}^A, \varphi_{m'}^A \right\rangle \right) n_{mm'}^\sigma n_{m''m'''}^\sigma \right\}. \quad (3) \end{aligned}$$

Here, V_{ee} is the screened electron-electron Coulomb repulsion. In the FLL formulation of E^{dc} seen in the Eq. 2, the parameters U and J, referred to as screened Coulomb and Hund's coupling parameters, enter as follows:

$$E^{dc}[n] = \frac{1}{2} U n(n-1) - \frac{1}{2} J [n^\uparrow (n^\uparrow - 1) + n^\downarrow (n^\downarrow - 1)] \quad (4)$$

In this formulation, which slightly differs from AMF, a constraint is applied to specific atomic orbitals of an atom. In practice, an energy constraint is applied to the Coulomb interaction between specific atomic orbitals of a chosen atom, preventing them from spreading over the entire structure. The LDA+U+J method shares similarities with the Hartree-Fock (HF) method. It essentially replaces certain electronic interactions with a Hamiltonian reminiscent of HF Hamiltonian, similar to hybrid functionals, where part of the functional involves a Fock exchange operator acting on KS states. However, LDA+U+J differs by utilising screened effective interactions and focusing only on a specific subset of states.

Within LDA+U+J an assumption of orbital independence is made due to the localised nature of the orbitals the correction is applied to. Despite its formal resemblance to HF, LDA+U+J operates on KS wave functions, lacking a direct physical interpretation beyond reproducing the charge density. In essence, LDA+U+J bridges concepts from HF and hybrid functionals, incorporating screened interactions and orbital decoupling while selectively applying corrections to specific states in the system.

Moreover, U and J can be construed as parameters representing the weight of an additional penalty function integrated into the total energy. This augmentation introduces a biased solution to DFT. The values of these parameters are intricately linked to the atomic environment and concentration of specific atoms relative to the overall quantity of atoms within the given structure. Their determination necessitates the application of one of four distinct methodologies: (i) fitting, wherein various properties such as lattice parameters or magnetic moments are juxtaposed for different U and J values at varying concentrations of strongly correlated atom types, (ii) the linear response approach, colloquially known as the Cococcioni-Gironcoli method [17, 18, 19], (iii) the constrained random phase approximation (cRPA) [20], or (iv) pseudohybrid Hubbard density functional ACBN0 [21]. Regrettably, (ii)-(iv) are notably intricate and do not always yield results close to experiment, and (i) cannot be employed *a priori* without experimental values for comparative analysis. Furthermore, as we demonstrate below, LDA+U+J fails to describe the charge and magnetic moment distribution correctly in some cases.

The U and J parameters play pivotal role in determining the magnetic moments (μ) of materials, particularly in systems characterised by strong electron-electron correlation and localised electronic states. These parameters influence magnetic moments through their effects on electronic configurations and spin alignments within the material's electronic structure.

1. **Hubbard U Parameter**:

   - The Hubbard U parameter characterises the on-site Coulomb repulsion between electrons occupying the same atomic orbital. It is quantified by the Hubbard Hamiltonian term:

   $$\hat{H}_U = U \sum_i \hat{n}_{i\uparrow} \hat{n}_{i\downarrow}$$

   where $\hat{n}_{i\sigma}$ represents the number operator for electrons with spin σ on site i.

   - Increasing U leads to a stronger repulsion between electrons on the same orbital, promoting electron localisation on different orbitals. This effect is captured by the Hubbard Hamiltonian.

   - In magnetic materials, localised electrons tend to align their spins to minimise the Coulomb repulsion energy, contributing to the material's magnetic moment. Therefore, larger values of U generally result in stronger electron localisation and larger magnetic moments.

2. **Hund's Coupling Parameter J**:

   - Hund's coupling J represents the exchange interaction between electrons with parallel spins on the same atomic site. It favours parallel spin configurations over anti parallel ones and is described by the Hamiltonian term:

   $$\hat{H}_J = -J \sum_i \left(\hat{S}_i^2 - \frac{\hat{n}_i(\hat{n}_i - 1)}{2} \right)$$

   where $\hat{S}_i$ is the total spin operator and $\hat{n}_i$ is the total electron number operator on site i.

   - Increasing J enhances the energy benefit of aligning spins, particularly in high-spin configurations with multiple unpaired electrons occupying orbitals with the same angular momentum (d- or f-orbitals), but different momentum projections m. This effect stabilises high-spin states and contributes to larger magnetic moments in magnetic materials.

3. **Interaction between U and J**:

   - U and J parameters often exhibit synergistic effects, where a larger U can enhance the effectiveness of J in stabilising high-spin states.

   - However, there can also be competing effects between U and J. For example, while larger values of U generally lead to more localised electron states and larger magnetic moments, excessively large U can hinder electron mobility and suppress magnetic ordering.

4. **Material-Specific Considerations**:

   - The influence of U and J parameters on magnetic moments depends on the material's specific electronic structure, crystal symmetry, and other material parameters.

   - Determination of U and J parameters tailored to the material of interest is essential for accurate predictions of magnetic properties. This can be achieved through empirical fitting or theoretical calculations based on electronic structure methods, as discussed above.

The above mentioned drawbacks can be overcome through the advanced potential-based self-consistency cDFT energy functional [22] denoted here as E^{cDFT}. This functional, designed to admit the same self-consistent solution as given by specific equations, is expressed as follows:

$$E^{\text{cDFT}}_{v_{\text{ext}}, N_A}[u] = E^v_{v_{\text{ext}}}[u] - R^v_A[u](W_{AA})^{-1} \left(\rho^v_A[u] - N_A \right) \quad (5)$$

Here, $E^v_{v_{\text{ext}}}[u]$ is the DFT energy, $R^v_A[u]$ is the residual self-consistent potential, W_{AA} is the overlap integral, u represents the screened potential, v_{ext} the external potential depending on atomic positions and cell parameters, and N_A the number of

Atom	x	y	z	LDA+U+J / μ_B	cDFT / μ_B
Ba	0.3333	0.6667	0.9816	-0.0003	0.0000
Ba	0.6667	0.3333	0.4816	-0.0003	0.0000
Y	0.3333	0.6667	0.3780	0.0037	0.0000
Y	0.6667	0.3333	0.8780	0.0037	0.0000
Co2	0.1692	0.3385	0.6908	2.4181	1.9974
Co2	0.6615	0.8308	0.6908	2.4181	1.9974
Co2	0.1692	0.8308	0.6908	2.4181	1.9974
Co2	0.8308	0.6615	0.1908	2.4181	1.9974
Co2	0.3385	0.1692	0.1908	2.4181	1.9974
Co2	0.8308	0.1692	0.1908	2.4181	1.9974
Co1	0.0000	0.0000	0.4423	-2.5309	-3.3055
Co1	0.0000	0.0000	0.9423	-2.5309	-3.3055
O	0.0091	0.5045	0.7642	0.0269	0.0000
O	0.4955	0.5045	0.7642	0.0269	0.0000
O	0.4955	0.9909	0.7642	0.0269	0.0000
O	0.9909	0.4955	0.2642	0.0269	0.0000
O	0.5045	0.4955	0.2642	0.0269	0.0000
O	0.5045	0.0091	0.2642	0.0269	0.0000
O	0.1634	0.3267	0.5033	-0.1161	0.0000
O	0.6733	0.8366	0.5033	-0.1161	0.0000
O	0.1634	0.8366	0.5033	-0.1161	0.0000
O	0.8366	0.6733	0.0033	-0.1161	0.0000
O	0.3267	0.1634	0.0033	-0.1161	0.0000
O	0.8366	0.1634	0.0033	-0.1161	0.0000
O	0.0000	0.0000	0.2571	-0.0658	0.0000
O	0.0000	0.0000	0.7571	-0.0658	0.0000

Table 1: Atomic fractional coordinates for the ferrimagnetic Y114 structure optimised with LDA+U+J (lattice parameters: $a = b = 6.274715382$ Å; $c = 10.234961467$ Å; $\alpha = \beta = 90$; $\gamma = 120$.)

electrons associated with a specific atomic fragment A. Notably, both v_{ext} and N_A are treated as external parameters in the calculation.

The functional $E_{v_{\text{ext}}, N_A}^{\text{cDFT}}[u]$ is stationary at the self-consistent potential v^*, leading to the following self-consistency relation:

$$E_{v_{\text{ext}}, N_A}^{\text{SC}} = E_{v_{\text{ext}}, N_A}^{\text{cDFT}}[v^*] \quad (6)$$

Moreover, the functional stationary behaviour is expressed as:

$$E_{v_{\text{ext}}, N_A}^{\text{cDFT}}[u] = E_{v_{\text{ext}}, N_A}^{\text{cDFT}}[v^*] + O((u - v^*)^2) \quad (7)$$

The gradient of this functional with respect to the screened potential u is given by:

$$\frac{\delta E_{v_{\text{ext}}, N_A}^{\text{cDFT}}[u]}{\delta u(\mathbf{r})} = \int \chi_0(\mathbf{r}, \mathbf{r}') R^{+v}[u, \Lambda_A[u]](\mathbf{r}') d\mathbf{r}' + \left(\int \epsilon_e(\mathbf{r}, \mathbf{r}') w_A(\mathbf{r}') d\mathbf{r}' \right) (W_{AA})^{-1} (\rho_A^v[u] - N_A) \quad (8)$$

Here, $\Lambda_A[u]$ is defined as:

$$\Lambda_A[u] \triangleq -R_A^v[u](W_{AA})^{-1}, \quad (9)$$

where $\epsilon_e(\mathbf{r}, \mathbf{r}')$ is the electron dielectric response function, and $\chi_0(\mathbf{r}, \mathbf{r}')$ is the independent-particle susceptibility. The formulation introduces a residual for cDFT, denoted as R^{cDFT}, defined as:

$$R^{\text{cDFT}}[u](\mathbf{r}') = R^{+v}[u, \Lambda_A[u]](\mathbf{r}') + c\, w_A(\mathbf{r}')\, (\rho_A[u] - N_A) \quad (10)$$

The residual vanishes when both R^{+v} and $\rho_A^v[u] - N_A$ vanish, indicating self-consistency.

The formulation allows for easy computation of derivatives and forces within the cDFT framework, using the $2n + 1$ theorem of perturbation theory. Notably, derivatives with respect to number of electrons (N_A) yield quantities such as the chemical potential of fragment A (χ_A).

The advantages of cDFT for describing magnetic moments are the following:

1. **Targeted Studies:** cDFT allows one to perform targeted studies by imposing specific constraints on the electronic density, such as fixing the magnetic moments of certain atoms or regions within a material. This capability is particularly useful for investigating phenomena like magnetic phase transitions, spin-crossover materials, or the effects of magnetic doping on electronic properties.

2. **Understanding Magnetism at the Atomic Level:** With cDFT, it is possible to explore the atomic-scale origins of magnetism in materials. By controlling the magnetic moments of individual atoms or groups of atoms, one can dissect the contributions of different electronic orbitals and chemical environments to the overall magnetic behaviour. This level of detail is crucial for understanding the microscopic mechanisms driving magnetic phenomena.

3. **Accurate Description of Magnetic Interactions:** Magnetic interactions play a fundamental role in determining the properties of magnetic materials. cDFT provides a rigorous framework for accurately describing these interactions by incorporating magnetic constraints directly into the electronic structure calculations. This ensures that magnetic interactions are treated self-consistently and accurately, leading to reliable predictions of magnetic ordering, magnetic anisotropy, and magnetic excitations.

4. **Prediction of Magnetic Properties:** By solving the electronic structure problem self-consistently within the constraints imposed by cDFT, one can obtain accurate predictions of various magnetic properties, such as magnetic moments, magnetic susceptibilities, and magnetic exchange interactions. These predictions can be compared with experimental measurements, providing valuable insights into the underlying physics of magnetism in materials.

5. **Exploration of Complex Magnetic Systems:** cDFT can be applied to explore the magnetic properties of complex systems, including magnetic nanoparticles, magnetic thin films, and magnetic heterostructures. These systems often exhibit intricate magnetic behaviours arising from size effects, interface effects, or proximity-induced magnetism. cDFT enables one to unravel these complexities
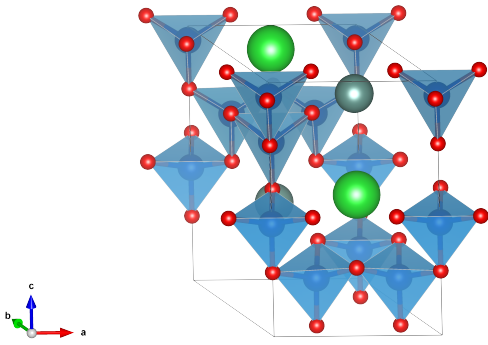
Figure 2: Crystal Structure of the optimised ferrimagnetic Y114

and understand how they influence the overall magnetic behaviour of the system.

6. **Design of New Magnetic Materials:** By leveraging the predictive capabilities of cDFT, one can accelerate the discovery and design of new magnetic materials with tailored magnetic properties. By systematically exploring the parameter space of different magnetic configurations, compositions, and structures, cDFT-guided computational screening can identify promising candidates for experimental synthesis and characterisation.

As a test example for cDFT theoretical framework, we investigate atomic and electronic structure, and magnetic interactions in Y114. Our choice of Y114 as a test case is strategic for several reasons. Firstly, its complex crystal structure and rich electronic properties make it an ideal candidate for exploring the interplay between electronic correlations, lattice distortions, and magnetic interactions. Additionally, the compound exhibits metallic behaviour with the drop of conductivity with increasing of temperature [23] and antiferromagnetic component at low temperature [1, 24, 5]. By utilising LDA+U+J and cDFT methods, we aim to capture the subtle interplay between electron-electron interactions and structural distortions that underlie the magnetism in Y114. These methods allow us to incorporate the effects of strong electron correlation and spin-orbit coupling, providing a more accurate description of the material's electronic structure compared to conventional DFT approximations.

Through comparative analysis of our theoretical predictions with experimental observations, we validate and refine our theoretical framework. In the future we expect to extend our investigation to other magnetic materials.

In essence, our study of the magnetism in Y114 serves is a stepping stone towards a more comprehensive theoretical understanding of complex materials, with implications for diverse fields ranging from condensed matter physics to materials science and beyond.

3. Computational Details

The atomic positions and lattice parameters of the hexagonal crystal structure of Y114 (Materials Project number: mp-1915155) are fully relaxed without spin-orbit coupling. This optimisation was executed in the plane-waves basis (PW) framework, employing the LDA+U+J energy functional [25, 12, 13, 14]. We have fitted the U and J parameters by comparing the computed lattice constants with those from neutron diffraction experiment on Y114 [1]. The final deviations from experimental values of lattice constants a and c were -0.27% and 0.34%, respectively, obtained with U = 8 eV for Co^{2+}, U = 6 eV for Co^{3+}, and J = 0.1 eV for both Co^{2+} and Co^{3+} with slightly different tetrahedral coordination. Potential-based self-consistent cDFT [7] with the LDA functional without spin-orbit coupling was used to self-consistently optimise the magnetic moments for the previously optimised ferrimagnetic structure with Hubbard model (see Fig. 1) constraining the charge of cobalt atoms to +3 and +2 for corresponding coordinations, and magnetic moments of Y, Ba, and O to zero. The atomic radii of 2.00 Bohr were chosen to solve the spherical integral around an atoms. These values are subjected to a smearing that will make the integral to go smoothly from 1 to 0 in the region from 1.8 to 2.0 Bohr avoiding the overlap between the atomic spheres. This type of partitioning is specific for optimised norm-conserving Vanderbilt pseudopotentials (ON-CVPs), which were taken from PseudoDojo project [26, 27] `pseudo-dojo.org`. The PW kinetic energy cut-off was set at 50 Ha, with a 6×6×3 Γ-centered k-point grid. Convergence was reached when forces fell below $5 \cdot 10^{-5}$ Ha/Bohr. For the geometry optimisation with LDA+U+J we used Quantum Espresso v.7.2 [28, 29], while cDFT calculations were executed utilising the `ABINIT` code [30, 31, 32].

4. Results and Discussion

We fully relaxed the hexagonal structure of Y114 with the ferrimagnetic order, adjusting both atomic positions and lattice constants, characterised by space group $P6_3mc$. Several optimisations were conducted using the LDA+U+J approach, applying different values of U and J on a grid to the 3d-electrons of Co ions. This iterative process aimed to determine the optimal U and J values that align the computed lattice constants with the experimental values obtained via neutron diffraction at 10 K, as reported in the literature [1], see the Computational Details section.

The Y114 crystal with the ferrimagnetic order exhibits two slightly different environments for Co^{2+} to Co^{3+} as seen in Fig. 2. This was not possible to observe in some experiments due to the electron delocalisation between cobalt sites, inducing fluctuations in the Co oxidation states from Co^{2+} to Co^{3+} and vice versa[1, 5, 33, 24]. According to our LDA+U+J calculations, Co ions in the two different oxidation states have the same oxygen coordination but slightly different Co-O bond lengths and angles in the O-tetrahedron. In the previous work by Tantardini *et al.* [6] a much more pronounced difference in coordination was observed for the two ions for the same structure but
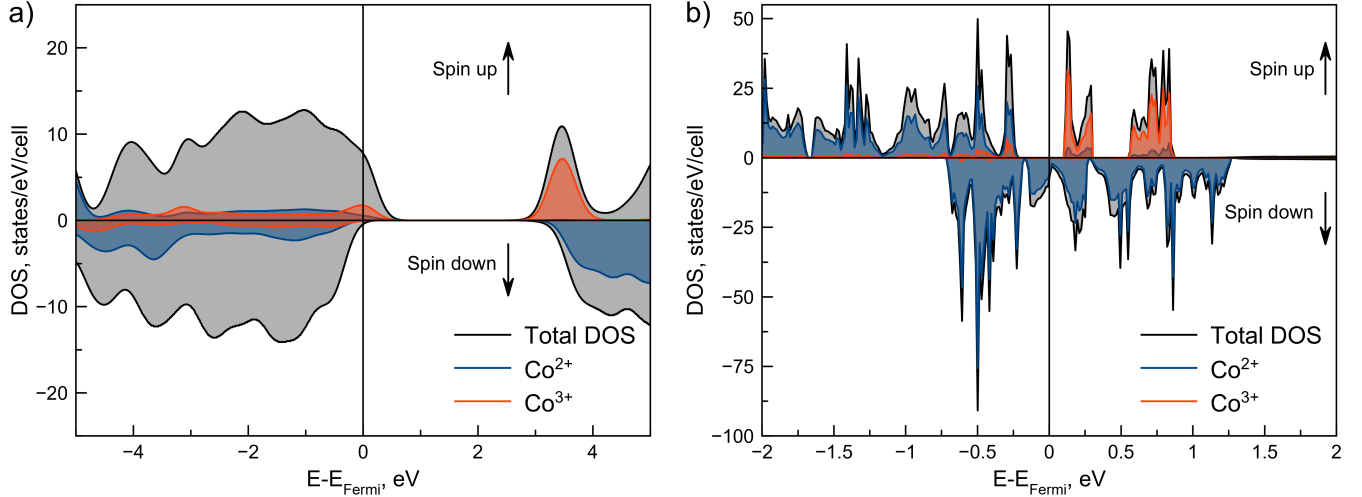
Figure 3: Total and Co 3d-projected density of states (pDOS) calculated with LDA+U+J (a) and cDFT (b).

in non polarised state: Co^{2+} coordination was trigonal, while Co^{3+} coordination remained tetrahedral.

Despite a slight deviation from the experimental values, our study successfully describes the different atomic sites within the material. Cobalt atoms are arranged such that Co^{3+} sites are positioned between the triangles formed by Co^{2+} sites, characteristic of the Kagome lattice structure.

The ferrimagnetic properties of the structure (see Tab. 1) are due to distinct magnetic moments for the two types of Co sites. The 3d-orbital occupation of a free Co^{2+} is 7, and the expected magnetic moments of Co^{2+} and Co $^{3+}$ in their high-spin states are therefore 3 μ_B and 4 μ_B, respectively. The LDA+U+J magnetic moments are 2.41 μ_B for Co^{2+} and -2.53 μ_B for Co^{3+}. The deviation between LDA+U+J magnetic moments and the expected values can be explained by a spillover of magnetic moment to other atoms in the crystal (e.g., oxygen), by Co ions adopting lower-spin states, by interaction between Co ions, or by a combination of these factors. We find a rather small magnetisation of the order of 0.1 μ_B on the oxygen atoms, which cannot explain the deviation. The experimental values of magnetic moments, deduced from inverse magnetic susceptibility measurement in X-ray powder diffraction at 2 K [5], are -3.49(8) μ_B for Co^{3+} and 2.19(4) μ_B for Co^{2+}. Interestingly, the experimental magnetic moment of Co^{2+} is even further from the expected high-spin moment 3 μ_B than the LDA+U+J, and falls almost exactly between the high-spin and low-spin value (1 μ_B) for the free Co^{2+} ion. As discussed in the literature on quantum chemical topology of spin-density distributions [34, 35], this can be explained by the interaction between Co ions in the lattice.

To address the discrepancies in magnetic moments derived from LDA+U+J and experiments, we employed cDFT [7] imposing a constraint on charge of the cobalt atoms. Based on the previous works [6, 1, 5, 33, 24], three of the four Co atoms per formula unit were assigned the oxidation state of +2, and the remaining Co atom was constrained to the oxidation state of

+3. Furthermore, oxygen barium, and yttrium are expected to be non-magnetic, and therefore their magnetic moments were constrained to be zero. It is note of worthy that cDFT predominantly accounts for local effects attributable to the different oxidation states of cobalt atoms, LDA+U+J incorporates long-range interactions originating from the projection of the KS states onto Co 3d-orbitals. cDFT yields the magnetic moments of -3.30 μ_B for Co^{3+} and 2.00 μ_B for Co^{2+}, which are much closer to the experimental values [5] than LDA+U+J (see Tab. 1). Thus, cDFT correctly reproduces the interaction (via chemical bonding) between Co ions, resulting in the apparent reduction of local spin moment on Co ions, particularly on Co^{2+} with (d^7) configuration.

These differences between LDA+U+J and cDFT are further investigated by examining the projected density of states (pDOS), as illustrated in Figure 3. We find drastic differences between the two methods. In contrast to LDA+U+J, which exhibits spin-majority states with predominant O 2p character at and near the Fermi energy (as depicted in Fig. 3a), cDFT pDOS in general exhibits sharper peaks, indicating state localisation, and the states around the Fermi level are spin-minority states with predominant Co^{2+} 3d character (Fig. 3b). The smaller contribution of O 2p states around the Fermi level in the case of cDFT can be attributed to the constraint steering the magnetic moments on non-magnetic ions in the crystal to zero. Thus, cDFT provides a unique and, according to the experimental results, more accurate representation of electronic structure and orbital occupation within Y114.

5. Conclusions

In this study, we have demonstrated how potential-based self-consistent cDFT can be used to improve description of magnetic interactions in complex magnetic compounds, using Y114 as a prototypical example. While LDA+U+J, with the parameters U and J fitted to reproduce experimental lattice constants,

6

correctly predicts charge disproportionation leading to slightly different tetrahedral O-coordination of Co^{2+} and Co^{3+} ions, and ferrimagnetic order, it fails to correctly describe magnetic moments of the Co ions. By imposing potential-based self-consistent charge constraints on the Co ions, and constraining the magnetic moments of non-magnetic ions (Y, Ba, and O) to be zero in the cDFT framework, we obtain magnetic moments of Co ions much closer to experimental values. Thus, potential-based self-consistent cDFT allows for accurate prediction of magnetic properties using the much more intuitive parameter choice (charges around the magnetic ions) than choice of U and J in LDA+U+J.

The cDFT results confirm the value of magnetic moment of Co^{2+} ions close to 2 μ_B, which is exactly between high-spin and low-spin states of an isolated Co^{2+} ion. This is explained by a strong interaction (bonding) between Co ions in the lattice. This bonding can also explain the dynamic redistribution of the +2/+3 charge in the Co lattice and the resulting oxygen tetrahedra distortion, rendering it difficult to detect in experiments.

6. Acknowledgments

References

[1] M. Valldor, M. Andersson, The structure of the new compound ybaco4o7 with a magnetic feature, Solid State Sciences 4 (7) (2002) 923–931.

[2] A. Maignan, V. Caignaert, D. Pelloquin, S. Hébert, V. Pralong, J. Hejtmanek, D. Khomskii, Spin, charge, and lattice coupling in triangular and kagomé sublattices of co o 4 tetrahedra: Yb ba co 4 o 7+ δ (δ= 0, 1), Physical Review B 74 (16) (2006) 165110.

[3] V. Caignaert, A. Maignan, V. Pralong, S. Hébert, D. Pelloquin, A cobaltite with a room temperature electrical and magnetic transition: Ybaco4o7, Solid state sciences 8 (10) (2006) 1160–1163.

[4] N. Podberezskaya, A. Smolentsev, L. Kozeeva, M. Y. Kameneva, A. Lavrov, Yttrium barium heptaoxocobaltate ybaco 4 o 7+ δ: Refinement of the structure and determination of the composition, Crystallography Reports 58 (2013) 682–686.

[5] L. Chapon, P. Radaelli, H. Zheng, J. Mitchell, Competing magnetic interactions in the extended kagomé system y ba co 4 o 7, Physical Review B 74 (17) (2006) 172401.

[6] C. Tantardini, E. Benassi, Crystal structure resolution of an insulator due to the cooperative jahn–teller effect through bader's theory: the challenging case of cobaltite oxide y114, Dalton Transactions 47 (15) (2018) 5483–5491.

[7] X. Gonze, B. Seddon, J. A. Elliott, C. Tantardini, A. V. Shapeev, Constrained density functional theory: A potential-based self-consistency approach, Journal of Chemical Theory and Computation 18 (10) (2022) 6099–6110.

[8] B. Kaduk, T. Kowalczyk, T. Van Voorhis, Constrained density functional theory, Chemical reviews 112 (1) (2012) 321–370.

[9] D. D. O'Regan, G. Teobaldi, Optimization of constrained density functional theory, Physical Review B 94 (3) (2016) 035159.

[10] Q. Wu, T. Van Voorhis, Constrained density functional theory and its application in long-range electron transfer, Journal of Chemical Theory and Computation 2 (3) (2006) 765–774.

[11] B. Himmetoglu, A. Floris, S. de Gironcoli, M. Cococcioni, Hubbard-corrected dft energy functionals: The lda+u description of correlated systems, International Journal of Quantum Chemistry 114 (1) (2014) 14–49.

[12] V. I. Anisimov, J. Zaanen, O. K. Andersen, Band theory and mott insulators: Hubbard u instead of stoner i, Physical Review B 44 (3) (1991) 943.

[13] V. Anisimov, O. Gunnarsson, Density-functional calculation of effective coulomb interactions in metals, Physical Review B 43 (10) (1991) 7570.

[14] V. I. Anisimov, I. V. Solovyev, M. A. Korotin, M. T. Czyżyk, G. A. Sawatzky, Density-functional theory and nio photoemission spectra, Phys. Rev. B 48 (1993) 16929–16934. doi:10.1103/PhysRevB.48.16929.
URL https://link.aps.org/doi/10.1103/PhysRevB.48.16929

[15] A. I. Liechtenstein, V. I. Anisimov, J. Zaanen, Density-functional theory and strong interactions: Orbital ordering in mott-hubbard insulators, Phys. Rev. B 52 (8) (1995) R5467–R5470. doi:10.1103/physrevb.52.r5467.
URL https://doi.org/10.1103/physrevb.52.r5467

[16] M. T. Czyżyk, G. A. Sawatzky, Local-density functional and on-site correlations: The electronic structure of la2cuo4 and lacuo3, Phys. Rev. B 49 (20) (1994) 14211–14228. doi:10.1103/physrevb.49.14211.
URL https://doi.org/10.1103/physrevb.49.14211

[17] M. Cococcioni, S. De Gironcoli, Linear response approach to the calculation of the effective interaction parameters in the lda+ u method, Physical Review B 71 (3) (2005) 035105.

[18] I. Timrov, N. Marzari, M. Cococcioni, Hp – a code for the calculation of hubbard parameters using density-functional perturbation theory, Computer Physics Communications 279 (2022) 108455.

[19] I. Timrov, N. Marzari, M. Cococcioni, Self-consistent hubbard parameters from density-functional perturbation theory in the ultrasoft and projector-augmented wave formulations, Phys. Rev. B 103 (2021) 045141. doi:10.1103/PhysRevB.103.045141.
URL https://link.aps.org/doi/10.1103/PhysRevB.103.045141

[20] B. Amadon, T. Applencourt, F. Bruneval, Screened coulomb interaction calculations: Crpa implementation and applications to dynamical screening and self-consistency in uranium dioxide and cerium, Phys. Rev. B 89 (12) (2014) 125110. doi:10.1103/physrevb.89.125110.
URL https://doi.org/10.1103/physrevb.89.125110

[21] L. A. Agapito, S. Curtarolo, M. Buongiorno Nardelli, Reformulation of DFT + u as a pseudohybrid hubbard density functional for accelerated materials discovery, Phys. Rev. X 5 (2015) 011006. doi:10.1103/PhysRevX.5.011006.
URL https://link.aps.org/doi/10.1103/PhysRevX.5.011006

[22] X. Gonze, B. Seddon, J. A. Elliott, C. Tantardini, A. V. Shapeev, Constrained density functional theory: A potential-based self-consistency approach, Journal of Chemical Theory and Computation 18 (10) (2022) 6099–6110.

[23] E. Tsipis, D. Khalyavin, S. Shiryaev, K. Redkina, P. Nunez, Electrical and magnetic properties of ybaco4o7+ δ, Materials chemistry and physics 92 (1) (2005) 33–38.

[24] A. Huq, J. Mitchell, H. Zheng, L. Chapon, P. Radaelli, K. Knight, P. Stephens, Structural and magnetic properties of the kagomé antiferromagnet ybbaco4o7, Journal of Solid State Chemistry 179 (4) (2006) 1136–1145.

[25] J. P. Perdew, Y. Wang, Accurate and simple analytic representation of the electron-gas correlation energy, Phys. Rev. B 45 (23) (1992) 13244–13249. doi:10.1103/physrevb.45.13244.
URL http://dx.doi.org/10.1103/physrevb.45.13244

[26] M. van Setten, M. Giantomassi, E. Bousquet, M. Verstraete, D. Hamann, X. Gonze, G.-M. Rignanese, The pseudodojo: Training and grading a 85 element optimized norm-conserving pseudopotential table, Computer Physics Communications 226 (2018) 39–54. doi:https://doi.org/10.1016/j.cpc.2018.01.012.
URL https://www.sciencedirect.com/science/article/pii/S0010465518300250

[27] D. R. Hamann, Optimized norm-conserving vanderbilt pseudopotentials, Phys. Rev. B 88 (2013) 085117.

[28] P. Giannozzi, S. Baroni, N. Bonini, M. Calandra, R. Car, C. Cavazzoni, D. Ceresoli, G. L. Chiarotti, M. Cococcioni, I. Dabo, A. D. Corso, S. de Gironcoli, S. Fabris, G. Fratesi, R. Gebauer, U. Gerstmann, C. Gougoussis, A. Kokalj, M. Lazzeri, L. Martin-Samos, N. Marzari, F. Mauri, R. Mazzarello, S. Paolini, A. Pasquarello, L. Paulatto, C. Sbraccia, S. Scandolo, G. Sclauzero, A. P. Seitsonen, A. Smogunov, P. Umari,

R. M. Wentzcovitch, Quantum espresso: a modular and open-source software project for quantum simulations of materials, Journal of Physics: Condensed Matter 21 (39) (2009) 395502.

[29] P. Giannozzi, O. Andreussi, T. Brumme, O. Bunau, M. B. Nardelli, M. Calandra, R. Car, C. Cavazzoni, D. Ceresoli, M. Cococcioni, N. Colonna, I. Carnimeo, A. D. Corso, S. de Gironcoli, P. Delugas, R. A. DiStasio, A. Ferretti, A. Floris, G. Fratesi, G. Fugallo, R. Gebauer, U. Gerstmann, F. Giustino, T. Gorni, J. Jia, M. Kawamura, H.-Y. Ko, A. Kokalj, E. Küçükbenli, M. Lazzeri, M. Marsili, N. Marzari, F. Mauri, N. L. Nguyen, H.-V. Nguyen, A. O. de-la Roza, L. Paulatto, S. Poncé, D. Rocca, R. Sabatini, B. Santra, M. Schlipf, A. P. Seitsonen, A. Smogunov, I. Timrov, T. Thonhauser, P. Umari, N. Vast, X. Wu, S. Baroni, Advanced capabilities for materials modelling with quantum espresso, Journal of Physics: Condensed Matter 29 (46) (2017) 465901.

[30] X. Gonze, F. Jollet, F. A. Araujo, D. Adams, B. Amadon, T. Applencourt, C. Audouze, J.-M. Beuken, J. Bieder, A. Bokhanchuk, E. Bousquet, F. Bruneval, D. Caliste, M. Côté, F. Dahm, F. D. Pieve, M. Delaveau, M. D. Gennaro, B. Dorado, C. Espejo, G. Geneste, L. Genovese, A. Gerossier, M. Giantomassi, Y. Gillet, D. Hamann, L. He, G. Jomard, J. L. Janssen, S. L. Roux, A. Levitt, A. Lherbier, F. Liu, I. Lukačević, A. Martin, C. Martins, M. Oliveira, S. Poncé, Y. Pouillon, T. Rangel, G.-M. Rignanese, A. Romero, B. Rousseau, O. Rubel, A. Shukri, M. Stankovski, M. Torrent, M. V. Setten, B. V. Troeye, M. Verstraete, D. Waroquiers, J. Wiktor, B. Xue, A. Zhou, J. Zwanziger, Recent developments in the abinit software package, Computer Physics Communications 205 (2016) 106–131.

[31] X. Gonze, B. Amadon, G. Antonius, F. Arnardi, L. Baguet, J.-M. Beuken, J. Bieder, F. Bottin, J. Bouchet, E. Bousquet, N. Brouwer, F. Bruneval, G. Brunin, T. Cavignac, J.-B. Charraud, W. Chen, M. Côté, S. Cottenier, J. Denier, G. Geneste, P. Ghosez, M. Giantomassi, Y. Gillet, O. Gingras, D. R. Hamann, G. Hautier, X. He, N. Helbig, N. Holzwarth, Y. Jia, F. Jollet, W. Lafargue-Dit-Hauret, K. Lejaeghere, M. A. L. Marques, A. Martin, C. Martins, H. P. C. Miranda, F. Naccarato, K. Persson, G. Petretto, V. Planes, Y. Pouillon, S. Prokhorenko, F. Ricci, G.-M. Rignanese, A. H. Romero, M. M. Schmitt, M. Torrent, M. J. van Setten, B. Van Troeye, M. J. Verstraete, G. Zérah, J. W. Zwanziger, The abinit project: Impact, environment and recent developments., Computer Physics Communications 248 (2020) 107042.

[32] A. H. Romero, D. C. Allan, B. Amadon, G. Antonius, T. Applencourt, L. Baguet, J. Bieder, F. Bottin, J. Bouchet, E. Bousquet, F. Bruneval, G. Brunin, D. Caliste, M. Côté, J. Denier, C. Dreyer, P. Ghosez, M. Giantomassi, Y. Gillet, O. Gingras, D. R. Hamann, G. Hautier, F. Jollet, G. Jomard, A. Martin, H. P. C. Miranda, F. Naccarato, G. Petretto, N. A. Pike, V. Planes, S. Prokhorenko, T. Rangel, F. Ricci, G.-M. Rignanese, M. Royo, M. Stengel, M. Torrent, M. J. van Setten, B. V. Troeye, M. J. Verstraete, J. Wiktor, J. W. Zwanziger, X. Gonze, Abinit: Overview, and focus on selected capabilities, J. Chem. Phys. 152 (2020) 124102.

[33] M. Soda, Y. Yasui, T. Moyoshi, M. Sato, N. Igawa, K. Kakurai, Magnetic structure of ybaco4o7 with kagome and triangular lattices, Journal of the Physical Society of Japan 75 (5) (2006) 054707.

[34] G. Bruno, G. Macetti, L. Lo Presti, C. Gatti, Spin density topology, Molecules 25 (15) (2020) 3537.

[35] G. Macetti, L. Lo Presti, C. Gatti, Spin density accuracy and distribution in azido cu (ii) complexes: A source function analysis, Journal of computational chemistry 39 (10) (2018) 587–603.